https://doi.org/10.5194/egusphere-2025-6509
Preprint. Discussion started: 10 February 2026

Frazil ice formation as a pathway for iron enrichment in Antarctic sea ice

Letizia Tedesco[1], Delphine Lannuzel[2,3,4], Julie Janssen[5], Lars H. Smedsrud[6]

[1]Marine and Freshwater Solutions, Finnish Environment Institute, Helsinki, Finland
[2]Institute for Marine and Antarctic Studies, University of Tasmania, Hobart, Australia
[3]Australian Antarctic Program Partnership, Institute for Marine and Antarctic Studies, University of Tasmania, nipaluna Hobart, TAS, Australia.
[4]Australian Centre for Excellence in Antarctic Science, Institute for Marine and Antarctic Studies, University of Tasmania, nipaluna Hobart, TAS, Australia.
[5]National Collections and Marine Infrastructure, Commonwealth Scientific and Industrial Research Organisation, Hobart, Australia.
[6]Geophysical Institute & Bjerknes Centre for Climate Research, University of Bergen, Norway.

Correspondence to: Letizia Tedesco (letizia.tedesco@environment.fi)

Abstract. The Southern Ocean plays a vital role in regulating Earth's climate by absorbing large quantities of carbon dioxide, but its productivity is strongly limited by the availability of iron needed for phytoplankton growth. Sea ice is a crucial seasonal reservoir of iron; however, the processes responsible for its enrichment remain poorly understood. Here we use a process-based model to show that frazil ice formation, a common feature of winter sea-ice growth in the Southern Ocean, can scavenge dissolved iron from seawater and concentrate it in newly formed ice. First-order estimates scaled to the Antarctic sea-ice zone suggest that frazil-origin ice could supply ~16–33% of the seasonal dissolved iron pool in the upper 10 m. Because this iron is released as a short-lived but intense pulse upon melt, frazil ice provides a pathway that can trigger phytoplankton blooms, linking polar sea-ice processes directly to global carbon cycling.

1 Introduction

The Southern Ocean is a globally significant carbon sink, accounting for 20–30% of the global biological carbon export (Boyd et al., 2024). However, this large contribution is partly constrained by Antarctic waters being rich in macronutrients but comparatively low in chlorophyll concentrations over 80% of the Southern Ocean, i.e., the high-nutrient low-chlorophyll (HNLC) puzzle (Martin et al., 1990). Iron (Fe) is an essential micronutrient for phytoplankton growth since it regulates chlorophyll synthesis and several key metabolic processes. Dissolved iron (dFe, <0.2µm) is the bioavailable form that limits phytoplankton growth in large areas of the ocean, while particulate iron (pFe, >0.2 µm) is generally less available, though some forms can be labile. Large parts of the Southern Ocean exhibit Fe levels that are generally too low in surface waters to allow phytoplankton growth (Martin et al., 1990). This low Fe availability is due to the low solubility of Fe in oxygenated

https://doi.org/10.5194/egusphere-2025-6509
Preprint. Discussion started: 10 February 2026

waters as well as the remoteness of the Southern Ocean from atmospheric and terrestrial Fe sources. The main sources of Fe in the Southern Ocean surface waters are sediment resuspension and upwelling (de Jong et al., 2013), melting glaciers (Death et al., 2014; Gerringa et al., 2012), icebergs (Duprat et al., 2016), and sea ice (Lannuzel et al., 2010) (Fig. 1).

Sea ice is considered one of the most important sources of Fe to the Southern Ocean's surface waters in spring, serving as a seasonal reservoir that transports Fe from coastal to offshore regions and triggers ice-edge phytoplankton blooms when it melts (Arrigo et al., 1997; Sedwick and DiTullio, 1997). Concentrations of dFe have been found at least one order of magnitude larger in sea ice than in typical Antarctic surface waters, i.e., 9.8 ± 15.0 nmol L^{-1} in sea ice (values spanning both frazil and congelation types, Lannuzel et al., 2016; Tedesco and Lannuzel, 2023) in comparison to 0.38 ± 0.55 nmol L^{-1} in seawater (Tagliabue et al., 2012). The enrichment in sea ice is also reported for Chlorophyll-a (Chl-a), particulate organic carbon (POC), and pFe, especially at the ice/water interface (Tedesco and Lannuzel, 2023). This suggests that seawater is the main source of this enrichment, although the mechanisms for Fe incorporation in sea ice remain elusive. A suite of processes has been suggested (Lannuzel et al., 2016).

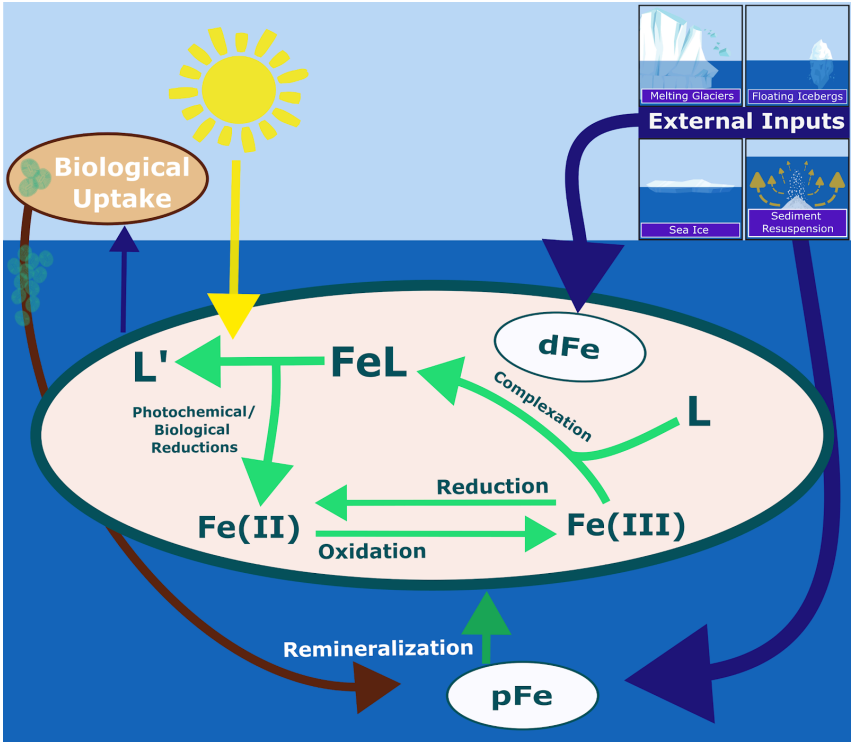

Figure 1: The iron cycle in surface waters of the Southern Ocean with a focus on the dissolved fraction (dFe). The external input of iron (Fe) to the surface waters of the Southern Ocean includes melting glaciers, icebergs, sediment resuspension, and sea ice.

https://doi.org/10.5194/egusphere-2025-6509
Preprint. Discussion started: 10 February 2026

Iron enrichment in sea ice is more pronounced in winter than in other seasons. During winter, all forms of particulate matter, including pFe, are enriched in sea ice compared to seawater from the early stages of ice formation (Janssen et al., 2018). To a lesser extent, dFe is also enriched, suggesting particle size influences impurity incorporation. Low Chl-a concentrations and lack of macronutrient drawdown indicate low biological activity in winter. Therefore, physical processes have been deemed the main mechanisms for the enrichment of dFe, pFe, and organic matter in newly formed sea ice, with pFe and dFe potentially decoupling during ice formation.

Within the dissolved fraction, ligands, potentially in the form of exopolysaccharides (EPS), are thought to control the distribution of dFe in sea ice by complexing iron or promoting bacterial remineralization of pFe into dFe (van der Merwe et al., 2009). During freezing, EPS would aid dFe adsorption to sea ice and, therefore, would be a crucial vector of dFe incorporation in forming sea ice (Lannuzel et al., 2015; Genovese et al., 2022). Within the particulate fraction, the co-occurrence of high pFe and POC in sea ice in winter has suggested co-scavenging from the water column (Lannuzel et al., 2007).

Understanding the conditions (e.g., turbulent versus calm) under which sea ice forms is key to understanding the pathways of Fe incorporation in sea ice. The majority of Antarctic sea ice is characterized by frazil ice underlain by congelation growth, with the proportion of granular (frazil) versus columnar (congelation) ice varying regionally and seasonally (Lange and Eicken, 1991). Congelation ice forms in calm, stable conditions (e.g., consolidated pack ice or refrozen leads), allowing crystals to grow vertically as heat is gradually lost from the ice-ocean interface. The large and vertically aligned crystals exclude particles, resulting in significantly lower particle concentrations in columnar ice and thus acting as a barrier to particle incorporation. In contrast, frazil ice forms under turbulent conditions (e.g., in polynyas and the marginal ice zone) with ice crystals developing in the water column in supercooling conditions and later accumulating and consolidating near the ocean surface. Dynamic regions with high wave and wind activity form a higher fraction of granular ice.

Frazil ice crystals can use materials suspended in the water column as condensation nuclei and subsequently rise to the ocean surface, trapping them within the developing ice (Weeks and Ackley, 1982). It has also been suggested that the number of times an ice crystal encounters any particle will determine how much material gets entrained in sea ice (Garrison et al., 1989) and that smaller frazil ice crystal sizes correspond to rapid ice growth during strong katabatic wind episodes. In contrast, larger frazil ice crystals denote slower growth, and crystals in surface waters may finally aggregate into pancakes (Tison et al., 2020). Ice tank experiments confirmed the incorporation and enrichment of various Fe-bearing materials, such as silt, clay, sand-sized particles, diatoms, foraminifera, and plankton by rising frazil crystals (Reimnitz et al., 1993). However, the pathways for frazil ice entrapment of Fe have yet to be fully understood and quantified.

https://doi.org/10.5194/egusphere-2025-6509
Preprint. Discussion started: 10 February 2026

To date, only a few models have considered the role of sea ice as a source of Fe to surface waters using simple parameterizations, resulting in significant differences in the magnitude and spatial distribution of dFe in Antarctic sea ice (Lancelot et al., 2009; Wadley et al., 2014; Wang et al., 2014). Different formulations of Fe incorporation in growing sea ice have been tested within a global ocean-sea ice biogeochemical model, considering atmospheric dust deposition, sediment mobilization, and river input as Fe sources (Person et al., 2020). Formulating the dFe incorporation rate proportional to seawater dFe concentrations produced the closest agreement with field observations.

Our study focuses on:
i) dFe, the form of Fe that is more bioavailable to phytoplankton;
ii) the winter season, when biological activity is minimal, and changes in Fe concentrations are therefore due mainly to physical processes;
iii) frazil ice, the type of ice suggested to be responsible for the high iron enrichment in newly formed sea ice.

We combine state-of-the-art field, laboratory, and model-based knowledge of frazil ice formation and consolidation into pack ice, particle scavenging, and resuspension to provide a comprehensive quantitative description of dFe adsorption and entrainment into newly forming granular sea ice from a generalized model of particle aggregation onto ice crystals. This includes modelling seawater supercooling, frazil ice formation, the adsorption of dFe onto ice crystals, the rising velocities of the aggregates, the entrainment of dFe into grease ice, and consolidation into pack ice (Fig. 2). The model is general and can be applied in polynya and non-polynya regions. Field observations are used for comparison and model calibration of unresolved parameters. This study provides a process-based, proof-of-concept quantification of frazil-mediated iron enrichment.

2 Results

2.1 Evidence of iron enrichment

Measurements of Fe in Antarctic sea ice are scarce and mainly collected during spring and summer (Lannuzel et al., 2016; Tedesco and Lannuzel., 2023). To date, there are no Fe measurements in sea ice during autumn, and only one campaign, the AWECS (Antarctic Winter Ecosystem Climate Study) expedition, collected winter sea-ice samples for Fe analysis. Between June 8 and August 12, 2013, AWECS visited eleven pack ice stations in the Weddell Sea (Tison et al., 2017). Three stations (488, 489, and 496) were characterized by relatively thin ice (less than 50 cm) and a high granular ice fraction; these stations were therefore considered suitable for our model study. The main physical properties measured are presented in Table 1, while their ice texture and associated in-ice and under-ice Chl-a profiles are shown in Fig. 3. All ice stations exhibited water depths ranging from 3000 to 4000 m. At stations 488 and 489, the sea ice exhibited distinct layers of granular and columnar ice, influencing the Chl-a profiles with variations in enrichment in granular ice and depletion in columnar ice. In contrast,

https://doi.org/10.5194/egusphere-2025-6509
Preprint. Discussion started: 10 February 2026

station 496 had a consistently granular ice texture with higher overall Chl-a concentrations and an increase in Chl-a from top to bottom, indicating algae accumulation (Fig. 3).

Additional ice cores were collected for Fe analysis at stations 488, 489, and 496. Given the close proximity between ice cores collected for ice texture and those for Fe analysis, we assume a similar ice texture between cores taken at a given station. Concentrations of dFe were only measured in the bottom 0.1 m of the ice cores (Table 2), but we assume a similar vertical distribution to Chl-a (Fig. 3) based on previous studies (Lannuzel et al., 2016; Tedesco and Lannuzel., 2023). The measurements show a very high enrichment in sea ice relative to seawater for all measured variables (Table 2). During AWECS, dFe was enriched in sea ice by an order of magnitude compared to surface waters. The larger algal cells exhibited the highest enrichment, approximately two orders of magnitude higher than in seawater. In contrast, dissolved macronutrients exhibited overall conservative behavior (not shown), with concentrations generally following dilution curves aligned with salinity. Ammonia was the exception, showing some enrichment in sea ice that we attribute to remineralization. Using Chl-a to carbon conversion ratios typical for small and large algal cells (0.015 and 0.025, respectively, Tedesco et al., 2010), data indicate that ice algae represented a small portion (ranging 8.3 - 23.4%) of the total POC. Particulate organic carbon was therefore mainly composed of detritus at this time of the year, confirming the predominant physical nature of the processes responsible for the enrichment of Fe and POC in newly formed sea ice.

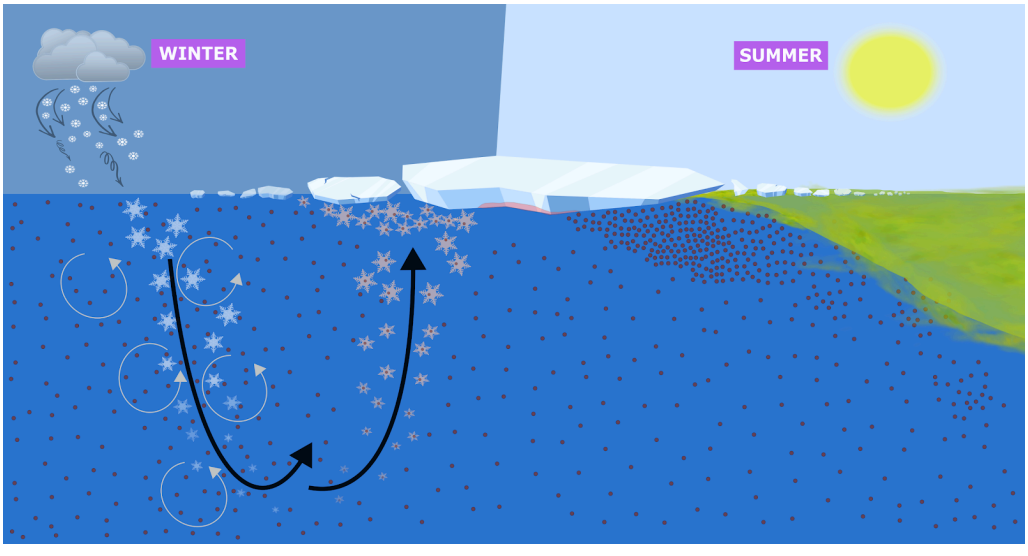

Figure 2: Schematic representation of the key processes contributing to the high iron enrichment in Antarctic sea ice. During winter, seawater supercooling leads to frazil ice formation, followed by the adsorption of dFe onto ice crystals. These aggregates rise through the water column and become entrained into grease ice, which eventually consolidates into pack ice. In summer, the melting of this ice releases iron into the surface ocean, supporting phytoplankton growth. Note: the schematic representation is not to scale.

https://doi.org/10.5194/egusphere-2025-6509
Preprint. Discussion started: 10 February 2026

2.2 A model for iron entrainment

Since the primary source of Fe in sea ice is seawater (Lannuzel et al., 2016), we consider the ocean the sole reservoir of Fe for sea ice, excluding any Fe input from atmospheric dust. Frazil ice crystals form in the water column (Martin, 1981), ranging in size from micrometers to centimeters. We approximate the continuous frazil ice size spectrum using five disk-shaped size classes k (Smedsrud, 2002), from small to large, with distinct diameter d_i, and rising velocities w_i (Table 3). In reality, frazil ice crystals often form needle-like or dendritic structures with high aspect ratios, much like snowflakes in the air. We represent these complicated crystals as disks, as this is a common, though idealized, approach for modeling suspended particles in any fluid. However, there are also no available observations of frazil crystal shape that could guide a more detailed approach.

We refer to dFe as one of the j sphere-shaped particle classes (Smedsrud, 2002). Knowing that the colloidal (0.02–0.2 µm) fraction represents 75% of the dissolved fraction on average, and 25% of dFe is in the soluble form (< 0.02 µm) (Lannuzel et al., 2014), we apply one size class to dFe with an average equivalent diameter of 0.1 µm. Our representation of these particles as spheres, while computationally efficient, does not capture their real geometry and should also be considered an idealization. According to Stokes' law (Stokes, 1851), the resulting velocity of dFe (~10^{-9} m s^{-1}) leads to a sinking depth of less than 1 mm per day. Therefore, we consider dFe neutrally buoyant and assign a zero settling velocity to dFe. The application of Stokes' Law to dFe particles is also a simplification. The drag and buoyancy forces on dFe particles and frazil crystals alike in nature may differ substantially from the theoretical Stokes' law. To estimate the potential of this process, we adopted a first-order approximation consistent with earlier aggregation models for frazil crystals and dFe particles.

Table 1: Seawater and sea-ice physical properties at AWECS stations. Surface seawater and average sea-ice physical properties of three thin ice and highly granular ice stations (488, 489, 496) sampled during the AWECS cruise in winter 2013.

	Station name	Station date	Station latitude	Station longitude		Snow depth (m)	Ice thickness (m)	Brine volume (%)	Temp (deg C)	Brine salinity ()	Salinity ()	Average wind speed (m s^{-1})
Semi-consolidated pancake ice	488	18.06.2013	62°.54S	00°.00W	*Seawater*				-1.9		34.5	12.70
					Sea ice	0.020	0.37	7.0	-7.5	118.5	9.0	
Consolidated pancake	489	19.06.2013	63°.54S	00°.01W	*Seawater*				-1.9		34.8	9.50
					Sea ice	0.066	0.36	6.7	-5.9	96.5	6.8	
Thin ice	496	24.06.2013	67°.26S	00°.01W	*Seawater*				-1.8		34.2	8.70
					Sea ice	0.226	0.61	8.9	-4.0	68.9	7.3	

Under turbulent conditions, frazil ice forms from supercooled water (Smedsrud, 2001; Drucker et al., 2003), and the individual crystals grow over time as long as supercooling remains. When turbulence ceases, frazil ice crystals rise towards the surface where they accumulate, forming grease ice. When grease ice congeals, it gives sea ice a granular texture. For example, in the Weddell Sea, 35% of all sea ice has been found fully granular, 32% columnar, 22% intermediate

https://doi.org/10.5194/egusphere-2025-6509
Preprint. Discussion started: 10 February 2026

columnar/granular, and 11% consisting of platelets (Eicken and Lange, 1989). In comparison, in the Arctic, up to 18 % at most of all sea ice has been found granular (Eicken et al., 1995). Suspended individual frazil ice crystals typically form when the wind speed exceeds 8-10 m s^{-1} and have been recorded at depths down to 30-50 m (Ito et al., 2019; Thompson et al., 2020; Ito et al., 2021), depending on turbulence. Accordingly, we activate frazil ice formation in the model when seawater temperature falls below its freezing point and conditions are turbulent (i.e., wind speed > 8 m s^{-1}).

We assume grease ice in the Southern Ocean consists of 25% frazil ice and 75% seawater, similar to Arctic grease ice (Smedsrud and Skogseth, 2006). Consequently, some thermal properties (e.g., density) can be calculated as weighted averages between frazil ice and seawater concentrations. We also assume that seawater below sea ice is well mixed, with prevailing turbulence processes causing high levels of vertical downward diffusion of frazil ice crystals (Fig. 2). As we follow an ice flow and simulate vertical processes, horizontal ocean currents and sea-ice velocities are ignored. Field measurements conducted in an Arctic polynya showed that grease ice can reach a thickness of 1 m (Smedsrud and Skogseth, 2006). Consequently, under ongoing turbulent conditions with strong winds and waves, frazil ice continues to form and only accumulates at the surface once the turbulence subsides. When the wind ceases or open water areas become small, frazil ice crystals rise to the surface and become grease ice. In the presence of waves, this ice will turn into pancakes. We calculate the turbulence depth in the model using a typical 1-D (vertical) k-ε ocean turbulence model, based on wind speed and water column depth on a vertical grid of 0.1 m.

Table 2: Seawater and bottom sea-ice properties at AWECS stations. Seawater and bottom (10 cm) sea-ice physical and biogeochemical properties at stations 488, 489, and 496 of the AWECS cruise in winter 2013.

	Station name		Snow depth (m)	Ice thickness (m)	Brine volume (%)	Temp (deg C)	Brine salinity (-)	Salinity (-)	POC (µg l-1)	Chl a (µg l-1) > 10µm	0.8µm < Chl a (µg l-1) < 10µm	Tot Chl a (µg l-1)	dFe (nmol l-1)	pFe (nmol l-1)
Semi-consolidated pancake	488	*Seawater*				-1.9		34.5	48.34	0.03	0.03	0.05	0.20	0.91*
		Sea ice	0.01-0.02	0.30-0.37	6.2	-4.7	86.2	5.3	920.89	1.41	0.29	1.69	1.03	35.71
		Enrich. Index							***124***	***366***	***74***	***220***	***34***	***255***
Consolidated pancake	489	*Seawater*				-1.9		34.8	28.05	0.02	0.04	0.06	0.20*	0.91*
		Sea ice	0.03-0.07	0.30-0.36	9.3	-3.7	67.6	6.3	440.76	1.58	0.81	2.39	1.22	20.09
		Enrich.							***87***	***436***	***112***	***220***	***20***	***122***
Thin ice	496	*Seawater*				-1.8		34.2	10.87	0.01	0.01	0.01	0.33	0.91
		Sea ice	0.04-0.23	0.40-0.61	13.1	-3.4	63.6	8.3	190.56	14.35	1.09	15.43	1.93	29.14
		Enrich.							***72***	***10748***	***688***	***5299***	***24***	***132***

Aggregation is defined here as any process that causes dFe and frazil ice crystals to adhere and form aggregates. We use the equivalent radius to characterize the size of each aggregate and treat it as a sphere (Smedsrud, 2002). When a frazil ice crystal collides with a particle and aggregates, the aggregate hybrid might sink or rise. The positive or negative velocity of the five size categories of aggregates is computed by considering the forces acting on the hybrid particle due to its buoyancy and drag in seawater (Stokes' law). After calculating the total volume, mass, and average density for each size, we compute the net buoyancy force acting on the aggregate from the ice and particle densities and that of the surrounding water. If the net

https://doi.org/10.5194/egusphere-2025-6509
Preprint. Discussion started: 10 February 2026

force is positive, the aggregate rises; if it is negative, it sinks. The resulting velocities are presented in Table 3. Here, dFe represents a type of "particle" in its broader sense, which adsorbs to ice crystals of any of the five size categories. Because the rising velocity for dFe adsorbed onto the smallest ice crystals is very small (~10^{-6} m s^{-1}), these aggregates rise over very long timescales, and we do not compute the dynamics of this aggregate size class. Large differences in rise velocities are seen between aggregates of different frazil ice classes, with aggregates made of large ice crystals rising more than three orders of magnitude faster than aggregates made of smaller ice crystals (Table 3).

Once turbulence has ceased, ice crystals rise towards the surface to form grease ice that contains incorporated dFe. The number of collisions controlling the level of dFe incorporation is a function of the particles' concentrations and radius, turbulent dissipation rate, constant kinematic viscosity, and an aggregation factor α (Smoluchowski, 1917). The aggregation factor α represents the statistical chance of aggregation (i.e., the colliding and sticking together efficiency); it is independent of the particle size, but dependent on other properties such as particle surface and shape (stickiness). The aggregation factor α can range between 0 (no aggregation when particles collide) and 1 (always aggregation) and is set constant within the same size class. The aggregation factor α has been found to range between 0.0001 and 0.1 for various frazil crystal size classes (25 µm to 1.5 cm) and particles (1–600 µm) (Smedsrud, 2002). We tested a variety of α values within the same range to calibrate the collision efficiency between ice crystals and dFe (Fig. 4).

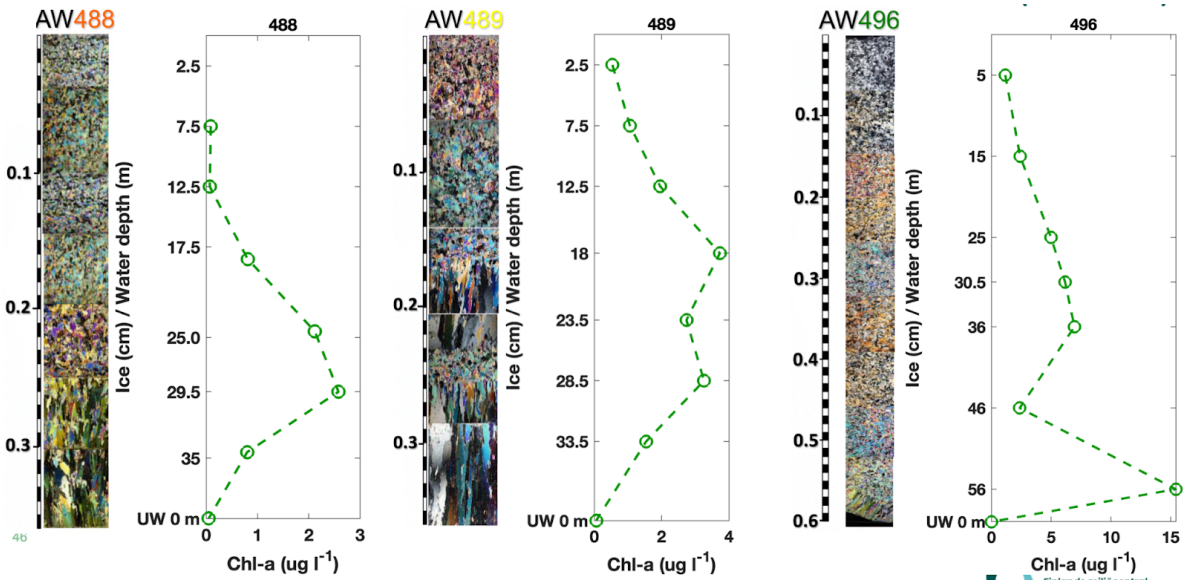

Figure 3: Selected ice cores' texture and associated Chl-a vertical profiles of the AWECS cruise in winter 2013. Textural characteristics of the AWECS13 ice cores 488 (left), 489 (middle), and 496 (right) with depth scale in meters (Tison et al., 2017), and associated Chl-a vertical profiles in sea-ice (depth in cm) and in under ice waters (i.e., UW 0 m). The thin sections are approximately 600 µm thick and were obtained using a microtome (Leica SM2400), following standard procedures. The sections were photographed between crossed polarizers, making the grain boundaries visible as color transitions due to different interference colors.

https://doi.org/10.5194/egusphere-2025-6509
Preprint. Discussion started: 10 February 2026

2.3 Numerical simulations of iron entrainment

We apply the model to simulate conditions similar to those observed at station 496 of AWECS because these are the only existing ice cores composed entirely of granular texture with analyzed dFe concentrations. We assume a constant seawater supercooling of 0.040°C, resulting from an atmospheric temperature well below the freezing point of seawater (-1.9°C), along with a wind speed of 8.7 m s^{-1}, as recorded on the sampling day (Table 1). A range of thresholds between $1e^{-3}$ and $1e^{-4}$ for both turbulent kinetic energy and dissipation rate yields a turbulence depth of approximately 22 to 30 m, consistent with observations (Ito et al., 2017). Because the water column is 4000 m deep, entrainment of water from below the surface mixed layer effectively acts as an infinite reservoir for dFe at a concentration of 0.330 nmol L^{-1}, matching measurements. An initial seeding volume concentration of crystals C_0 of 3.60×10^{-5} is introduced, corresponding to one hour of snowfall (1.0×10^{-8} m s^{-1}, with snow crystal diameter of 2.5 mm, Smedsrud, 2002). This seeding is equally distributed among the five ice crystal classes. The model is run for at least 1.5 days to ensure that all aggregates ascend, as the slowest aggregates, composed of fine crystals, take approximately 1.2 days to rise once turbulence subsides.

Table 3: Rise and sinking velocities of frazil ice and dFe. Top: Frazil ice classes (k) and related rise velocities (w), and rise depth in one hour. Middle: dFe properties and associated sinking velocity and sinking depth in one day. Bottom: Rise and sinking velocities (m s^{-1}) of the aggregates according to Stokes' law (Stokes, 1851). In brackets, the equivalent radius for ice crystals and dFe.

Frazil ice				
Class size k	*Range (median, d_i)*	*Equiv. radius (r_i, µm)*	*Rise velocity (w_i, mm/s)*	*Rise depth in 1 h (m)*
Small	0 - 50 µm (25 µm)	4.6	0.005	0.018
Fine	50-500 µm (250 µm)	46.0	0.054	0.194
Medium	0.5-5.0 mm (2.5 mm)	460.5	6.3	22.68
Coarse	5-10 mm (7.5 mm)	1381.5	21.2	76.32
Large	1-2 cm (1.5 cm)	2763.0	38.8	139.68
Iron				
Class size j	*Range (d_p, µm)*	*Median size (d_p, µm)*	*Sinking velocity (w_p, mm/s)*	*Sinking depth in 1 day (m)*
dFe	< 0.2	0.1	0	0
Rise velocity of aggregates				
Frazil ice →	*Fine (46.0 µm)*	*Medium (460.5 µm)*	*Coarse (1381.5 µm)*	*Large (2763.0 µm)*
Iron ↓				
dFe (0.05 µm)	2.8426e-04	0.0285	0.2564	1.0256

According to parameterizations of grease ice thickness and solidification (Smedsrud, 2011; Smedsrud and Martin, 2015, see also Methods), if the granular ice sampled at station 496 was already fully solidified, it might have originated from the freezing of about 0.8 m of grease ice. This formation could have occurred under an average wind speed of ~ 8.7 m s^{-1} (Table 1) and ocean currents of 0.7 m s^{-1}. Alternatively, if the freezing process were still ongoing, a grease ice thickness of about 0.6 m would have resulted in a solidified ice thickness of approximately 0.3 m, assuming the same wind intensity and ocean currents. To evaluate whether the environmental conditions at the site were favorable to frazil ice formation, we retrieved hourly wind speed and air temperature values from ERA5 (Hersbach et al., 2020) for the week before sampling. We found that air temperature was constantly below freezing, and the average wind speed was 7.3 m s^{-1}, and more than 50% of the time

https://doi.org/10.5194/egusphere-2025-6509
Preprint. Discussion started: 10 February 2026

above the 8.0 m s^{-1} threshold. We conclude that the environmental conditions at the site were consistent with the observed ice texture and thickness. Additionally, the parameterizations for grease ice thickness and solidification (Smedsrud, 2011; Smedsrud and Martin, 2015) were found to be directly applicable to Antarctic sea ice.

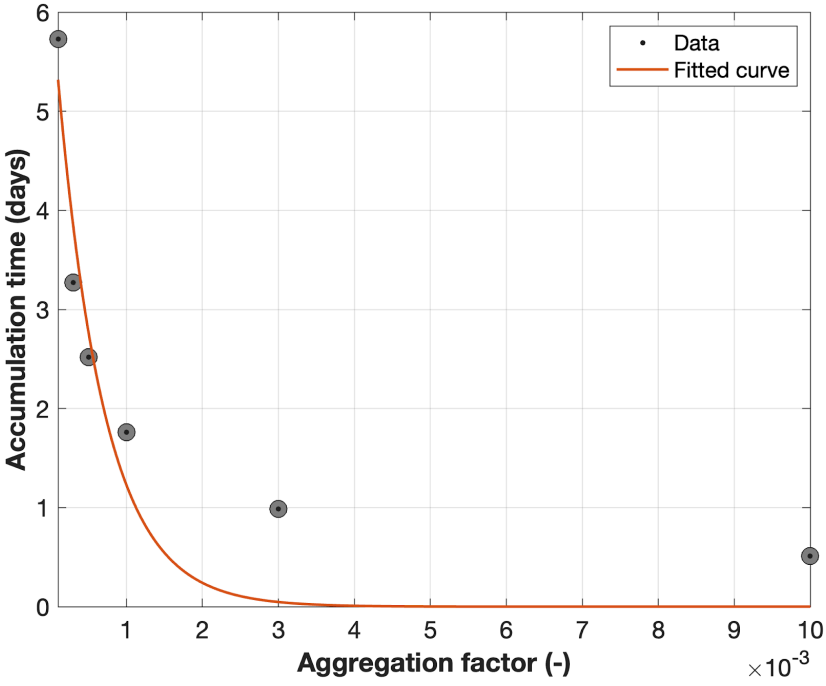

Figure 4: Model sensitivity to different values of the aggregation factor (α). Scatterplot showing the relationship between α (unitless) and the time (in days) required to reach the observed dFe concentration of 1.93 nmol L^{-1}. The red curve represents an exponential fit, illustrating the inverse relationship between α and accumulation time.

Running the model with the minimum aggregation factor (α = 0.0001, Smedsrud, 2002) results in the accumulation of dFe in sea ice to observed levels (1.93 nmol dFe L^{-1}) within just under 6 days (Fig. 4), a plausible timescale under conditions of sustained turbulence. Increasing α by an order of magnitude (to 0.001) accelerates this process, reaching the same concentration in just under 2 days (Fig. 4), which remains realistic and would allow for the full rise of aggregates. Further increasing α by another order of magnitude (to 0.01) leads to a rapid accumulation within approximately half a day (Fig. 4), which is probably unrealistic, as it may not permit sufficient time for effective dFe enrichment. Based on this analysis, we constrain plausible values for α to a range between the previously proposed minimum (0.0001, Smedsrud, 2002) and 0.001. Slightly lower or higher values may still be applicable. Our sensitivity analysis narrows down suitable values of the aggregation factor α specifically for dFe. An intermediate aggregation factor (α = 0.0005) enables dFe accumulation in just over two and a half days of sustained turbulence, frazil ice formation, and particle collision (Fig. 4) — a highly realistic timeframe. Under these conditions, the model yields a cumulative volume concentration of frazil ice crystals (C_i) ranging

https://doi.org/10.5194/egusphere-2025-6509
Preprint. Discussion started: 10 February 2026

from 2.01 × 10^{-5} (k_2) to 1.3 × 10^{-3} (k_5), with corresponding dFe concentration of 0.02 nmol l^{-1} and 1.18 nmol l^{-1}, respectively, highlighting the dominant contribution of larger crystals. When the model is constrained to a single-size class of frazil ice crystals with an equivalent radius of 5 mm, similar dFe levels are achieved (1.82 nmol dFe l^{-1}), suggesting the potential for model simplification in large-scale applications. It is important to note that α was here constrained empirically to reproduce the observed enrichment and was forced by average atmospheric conditions from reanalysis products. While this produces plausible values for α under these specific conditions, it might not represent a universal constraint on Antarctic-wide processes.

3. Discussion and Conclusions

The Southern Ocean's seasonal ice zone sees rapid sea-ice growth of several million km^2 each year, much of which begins as frazil ice. Frazil ice formation peaks during the winter months (June to September). In this season, temperatures drop significantly, and the winds strengthen, especially creating open water conditions in coastal polynyas, critical areas for frazil ice formation, where 10% of the Southern Ocean's sea-ice production occurs (Tamura et al., 2008). While frazil ice accounts for typically less than 10% of the total sea-ice production in non-polynya regions, it can represent up to 80% in polynyas (Gow et al, 1982; Thompson et al., 2020). This suggests that frazil ice formation plays a crucial role in iron enrichment within these sea-ice environments.

Sea-ice extent in the Southern Ocean has shown significant interannual variability in recent decades (Parkinson, 2019). In 2014, Antarctic sea ice reached a record-high winter maximum extent of ~20.1 million km², following a relatively large summer minimum of ~3.5 million km². This was the fourth-largest summer extent on record in the satellite era, but resulted in ~16.6 million km² of new sea ice production. In contrast, 2023 recorded the lowest winter maximum ever observed at ~17.0 million km², preceded by the lowest summer minimum of just ~1.8 million km², yielding ~15.2 million km² of new sea ice. Satellite altimetry and model-based estimates indicate that average winter sea-ice thickness was also greater in 2014 (~1.2 m, Fons et al., 2023) compared to 2023 (~1.0 m, Josey et al., 2024). These differences in both extent and thickness mirror broader climate system changes, with 2014 dominated by cold atmospheric conditions and strong offshore winds favorable for ice formation, whereas 2023 experienced warmer ocean and air temperatures, anomalous circulation patterns, and reduced ice production and retention.

Year-round observational and modelling studies consistently indicate that a substantial fraction, typically 30-50%, of Antarctic sea ice originates as frazil ice, especially within coastal polynyas and leads (Ohshima et al., 2022; Wilchinsky et al., 2015). Ice-core texture analyses conducted during the freezing season (April–September) across multiple Antarctic sectors — including the Weddell, Ross, Bellingshausen, and Amundsen Seas — reveal that frazil-derived (granular) ice accounts for 44% to over 80% of total ice thickness, with some pancake ice cores classified as 100% granular (Gow et al., 1982; Lange and Eicken, 1991; Jeffries et al, 2015; Thompson et al., 2020; Skatulla et al., 2022). The contribution of

https://doi.org/10.5194/egusphere-2025-6509
Preprint. Discussion started: 10 February 2026

frazil-origin ice also varies interannually. Based on the numbers above, total winter sea-ice volume for a cold year like 2014 was ~19920 km³, with ice of frazil origin likely comprising ~50% (i.e., the highest value of the range), or ~9960 km³. In contrast, during the record-low ice year 2023, total winter volume declined to ~15170 km³, with sea ice of frazil origin likely accounting for ~30% (i.e., the lowest value of the range) or ~4550 km³. These should be considered first-order estimates rather than precise values. Extrapolation to all Antarctic environments should be cautious because consolidation pathways may differ between polynyas and marginal ice zone settings, potentially altering the extent of frazil incorporation.

Assuming an average dFe concentration of 0.38 nmol L^{-1} in surface waters of the Southern Ocean (Tagliabue et al., 2012), a single-size class of ice crystals with an equivalent radius of 5 mm, and an aggregation factor α of 0.005, our model simulates a winter dFe concentration in sea ice of 2.1 nmol L^{-1}. If these results are considered broadly representative of seasonally ice-covered Antarctic waters and integrated over the estimated frazil ice volumes, the contribution of frazil ice to the dFe pool is ~2.1 × 10^7 mol (~1.2 Gg) in a cold year like 2014 and ~0.95 × 10^7 mol (~0.5 Gg) in a warm year like 2023. These values may be up to one order of magnitude higher than previous estimates (Edwards and Sedwick, 2001) and suggest that the contribution of frazil ice may rival that of icebergs in some contexts (Raiswell et al., 2008).

Considering that Antarctic ice-covered waters would contain ~5.8 × 10^7 mol (~3.2 Gg) of dFe in the upper 10 m in a year like 2023, and ~6.3 × 10^7 mol (~3.2 Gg) in a year like 2014, the contribution from frazil-origin sea ice — representing 30-50% of total ice volume — could account for an injection of roughly 16-33% of the total dFe pool in the upper 10 m upon sea-ice melt. This iron-enriched input would be released rapidly, effectively acting as a short-lived pulse that can trigger phytoplankton blooms and serves as a dominant new iron source during early spring in the seasonal ice zone. By identifying frazil ice formation as a pathway for iron enrichment, this study contributes to understanding cryospheric ecosystem feedbacks under a changing climate.

Our sensitivity analysis focused on the aggregation factor α, the most uncertain parameter directly linking particle stickiness to frazil incorporation. However, other parameters such as turbulence depth, frazil crystal size distribution, and supercooling intensity are also expected to strongly influence enrichment. These were not systematically varied here; thus, our simulations should be interpreted as a process demonstration rather than a predictive Antarctic-scale quantification. Future model developments should include multi-parameter sensitivity studies, supported by targeted field campaigns, to establish how robust frazil scavenging is across the range of Antarctic environments.

As global temperatures continue to rise, projections indicate a decline in overall sea-ice extent in the Southern Ocean under all emission scenarios for the 21st century (Roach et al., 2020). As Antarctic sea ice continues to shrink, warmer ocean and atmospheric conditions are expected to also shorten the sea-ice season, thereby reducing opportunities for frazil ice formation, similar to what was observed during the winter of 2023. Specifically, with warming, fewer regions may

https://doi.org/10.5194/egusphere-2025-6509
Preprint. Discussion started: 10 February 2026

experience the cold temperatures necessary to sustain extensive frazil ice formation, especially during the early stages of the ice growth season. Wind-driven mixing is crucial for frazil ice formation, particularly in coastal polynyas, where strong winds create open water areas and turbulent conditions that are conducive to frazil ice growth. Climate models suggest that changes in wind patterns, such as the strengthening of the Southern Annular Mode (SAM) and shifts in atmospheric circulation, could alter polynya dynamics (Ayres et al., 2024; Zhang et al., 2024). A future with stronger winds could potentially maintain or even enhance polynya activity in certain regions, such as the Ross Sea and Weddell Sea, supporting continued frazil ice formation despite warmer conditions. The overall balance is uncertain and requires dedicated modelling and field studies. Nonetheless, it remains clear that, even during record-low sea-ice years, frazil ice-driven dFe enrichment is extensive and represents one important mechanism, alongside other physical and biogeochemical processes, contributing to the role of sea ice in the Southern Ocean iron cycle.

Our study focuses specifically on dFe incorporation in sea ice, as dFe is the form of iron that is most readily available for uptake by ice algae and phytoplankton. However, sea ice is often even more enriched in pFe, with typically higher concentrations compared to dFe (Tedesco and Lannuzel., 2023). One proposed mechanism for the high levels of pFe in thin and newly formed sea ice is the scavenging process, where suspended biogenic or lithogenic iron particles are captured by rising frazil ice crystals during their formation (Lannuzel et al., 2010). Our model quantifies this scavenging process by directly calculating the aggregation between ice and particles. This process is also similar to those suggested for incorporating algae into sea ice (Weeks and Ackley, 1982; Garrison et al., 1989). While pFe is not directly available for algal uptake, it can become bioavailable through bacterial remineralization, which converts particulate forms into dissolved forms suitable for algae. While our model focuses on dFe incorporation only, the pFe–Chl-a relationship can provide important complementary evidence that particle scavenging processes play a central role in enrichment, and underscores the need for future work to explicitly couple pFe and dFe dynamics in modelling efforts, as more field observations become available, since remineralization in sea ice is yet to be quantified in the field.

The new model for dFe entrainment described here relies on several empirical parameters and assumptions, primarily due to the extremely limited availability of observational data necessary for comprehensive model calibration and evaluation. To date, only one winter station has been found with sea ice of a fully granular texture that was sampled for Fe analysis. While the model is well grounded in established laboratory tests, field observations, and theoretical frameworks related to frazil ice formation, particle aggregation, and buoyancy dynamics in seawater, key aspects such as the complexities of the iron cycle, as well as the levels of turbulence, supercooling, and aggregation, require further work. For example, it should be emphasized that our model represents only the aggregation pathway of frazil–particle interactions, and that the treatment of crystals as disks and dFe as spherical ‘sticky particle’ is a simplification of their geometry. While this abstraction allows us to demonstrate the plausibility of frazil scavenging under observed conditions, it does not imply that the fundamental physics of crystal growth and particle scavenging are fully captured. Crystal shape effects and alternative incorporation pathways

https://doi.org/10.5194/egusphere-2025-6509
Preprint. Discussion started: 10 February 2026

represent important avenues for future work. While this study has reduced the uncertainty associated with the most unresolved parameter of the model, i.e., the aggregation factor α, to more extensively validate and develop the model, targeted winter field campaigns and laboratory studies are crucial to foster knowledge of the mechanisms underlying the high iron enrichment during sea-ice formation and cascading impacts on the Southern Ocean's carbon sink.

Methods

We define a Fe enrichment index I_{en} (Gradinger and Ikävalko, 1998) as:

$$I_{en} = \frac{S_w C_{xi}}{S_i C_{xw}}$$

Here, S_w is the seawater salinity and S_i sea-ice bulk salinity, and C_{xi} and C_{xw} are concentrations of the variable of interest (x) in sea ice and seawater, respectively. This estimates any enrichment in sea ice compared to seawater, scaled by the respective salinities.

We compute the potential settling velocities, w_p of dFe (Table 3), according to Stokes' law (33):

$$w_p = \frac{(\rho_w - \rho_p) g d_p^2}{9\mu_w}$$

where ρ_w and μ_w are the seawater density (1028 kg m^{-3}) and dynamic viscosity (2.044 × 10^{-3} kg m^{-1} s^{-1}), respectively, for seawater at -2°C temperature and 35 salinity (-), g is the acceleration due to gravity, and ρ_p is the particle density (2650 kg m^{-3}, typical of faecal pellets).

We compute the grease ice thickness h_g, considering both the drag from the wind U_a as well as the ocean current U_w in conditions of negligible ice motion (Smedsrud, 2011):

$$\overline{h_g} = \frac{2}{3}(V_g)^{\frac{1}{3}} \left[\sqrt{\frac{\rho_a C_a}{K_r}} U_a + \sqrt{\frac{\rho_w C_w}{K_r}} U_w \right]^{\frac{2}{3}}$$

where V_g is the grease ice volume per unit width (m^3 m^{-1}, calibrated value 40), ρ_a is the air density (1.3 kg m^{-3}), C_a and C_w are the air and ice-water drag coefficients (typically 1.3 × 10^{-3} and 5.5 × 10^{-3}, respectively, McPhee, 1975; Smith, 1988), and K_r is the resistance force towards packing (N m^{-3}, calibrated value 100, Smedsrud, 2011). In the absence of significant ocean currents, the right-hand side of the equation can be ignored, and the grease ice thickness becomes proportional only to $U_a^{2/3}$. This 'horizontal packing process' is rapid and will occur within a time scale of hours, and so, in our approach, it is thought of as instant. As the ice solidifies at the surface, it loses a significant portion of the seawater. We use a parameterization for

https://doi.org/10.5194/egusphere-2025-6509
Preprint. Discussion started: 10 February 2026

grease ice solidification h_p that is dependent on grease ice thickness h_g, bulk sea ice S_i, and seawater salinity S_w (Smedsrud and Martin, 2015):

$$\overline{h_p} = \frac{1}{4}\left(1 + \frac{S_i}{S_w}\frac{\rho_i + 3\rho_w}{\rho_w}\right)\overline{h_g}$$

The turbulence depth is determined as the depth at which both the turbulent kinetic energy and dissipation rate fall below a threshold value, which we set rather conservatively ($1e^{-3}$-$1e^{-4}$). We allow frazil ice to form and be uniformly distributed within this turbulent depth. If the computed turbulence depth exceeds the water column depth, an additional process responsible for bottom resuspension should be considered. This also applies to sites where bottom currents are known to be relevant.

In a well-mixed surface layer with high levels of turbulence, frazil ice and particle volume concentrations change in time following (Omstedt and Svensson, 1984):

$$\frac{\partial C_p(j)}{\partial t} = -w_p\frac{\partial C_p(j)}{\partial z}$$

$$\frac{\partial C_i(k)}{\partial t} = -w_i\frac{\partial C_i(k)}{\partial z} + G_i(k)$$

where C_p and C_i are the volume concentrations of particles of class j and frazil ice of class k, respectively, and w_p and w_i are the sinking and rising velocities of particles and frazil crystals, respectively (Table 3). If the water column depth is as deep as, for example, at station 496, we can consider the water column as an infinite reservoir of particles. Instead, G_i (s^{-1}) is a source/sink term for frazil ice:

$$G_i(k) = \frac{aC_i(k)Q_i(k)}{L_i\rho_w}$$

where a is the ratio of surface area to volume for the ice crystals, and L_i is the latent heat of crystallization for pure ice (3.35×10^5 J kg^{-1}). Assuming that crystals are disks (Sherwood, 2000; Smedsrud, 2002), the heat flux Q_i between the ice crystal and the surrounding waters is then:

$$Q_i(k) = \frac{N_u K_w(T_i - T_w)}{2r_i(k)}$$

https://doi.org/10.5194/egusphere-2025-6509
Preprint. Discussion started: 10 February 2026

Here $N_u \approx 6$ is the Nusselt number and r_i is the equivalent crystal radius (Table 3). The Nusselt number describes the ratio between the turbulent and conductive heat transfers (Thompson et al., 2020). $K_w \approx 0.564$ W m^{-1} °C^{-1} is the thermal conductivity at the ice/water interface, T_i is the frazil ice temperature, assumed to be at the freezing point of seawater, and T_w is the seawater temperature. The level of supercooling is difficult to observe accurately due to the presence of small frazil crystals, which can distort conductivity measurements. In the absence of such in-situ observations, we use a constant level of supercooling of 0.040°C (Skogseth et al., 2009). This level of supercooling is considered representative of situations with strong wind (>8 m s^{-1}) and large surface heat loss (Tamura et al., 2008). It is also comparable to the level of supercooling generally found in the surface mixed layer throughout the Southern Ocean during winter (Haumann et al., 2020). We apply this level of supercooling over the period when the frazil ice production is activated. The level of supercooling only determines when the frazil ice formation process starts, while the frazil ice volume is controlled by the surface heat flux. When frazil ice is not forming, the term Q_i is zero because T_w=T_i. Once frazil ice formation is triggered, the volume of frazil ice is determined by G_i, which is a function of the heat flux Q_i. Although the supercooling levels remain constant, the resulting heat flux into each ice crystal (Q_i) is not, depending on the equivalent radius of the ice crystals. The frazil ice source term, G_i, then varies only according to the ice crystal size, with smaller growth (G_i) for larger crystals and more effective growth for smaller crystals. No observations are available on turbulence levels, supercooling, and frazil crystal size, but it is expected that higher turbulence leads to the formation of smaller ice crystals due to increased collision and fragmentation (Garrison et al., 1989; Smedsrud, 2002). In contrast, under lower turbulence, crystals are less likely to break, allowing them to grow larger and rise more effectively toward the surface.

The number of collisions N_c controlling the dFe level between particles and ice crystals per unit time is given by Smoluchowski (1917):

$$Nc_{ip} \propto (r_i + r_p) n_i n_p$$

where ni and n_p are number concentrations. The change in the number of aggregates n_a is then (Smedsrud, 2002):

$$\frac{dn_a}{dt} = \alpha \frac{(r_i(k) + r_p(j))^3}{t_T} n_{i(k)} n_{p(j)}$$

where t_T is Taylor's time scale for turbulent strength (Tennekes and Lumley, 1994) $(15\ \upsilon\ \varepsilon^{-1})^{1/2}$, ε is the turbulent dissipation rate (2.0 × 10-8 W kg^{-1}), and υ is the constant kinematic viscosity (1.8 × 10^{-6} m^2 s^{-1}). The transfer to C_a is done by multiplying the corresponding spherical volumes.

https://doi.org/10.5194/egusphere-2025-6509
Preprint. Discussion started: 10 February 2026

Code and data availability

All data needed to evaluate the conclusions in the paper are present in the paper. Model code and simulations will be made available on an open digital repository upon acceptance of the manuscript.

Author contributions

LT and DL conceptualized the study with contributions from JJ. LT devised the methodology with contributions from LS. LT developed the model, carried out the analysis and wrote the original draft. All authors reviewed and edited the manuscript.

Competing interests

The authors declare no competing interests.

Acknowledgements

This work was written under the auspices of BEPSII (Biogeochemical Exchange Processes at the Sea-Ice Interfaces) Expert Group (www.bepsii.org).

Financial support

LT has received funding from the European Union's Horizon 2020 research and innovation program under Grant Agreement No. 101003826 via project CRiceS (Climate Relevant interactions and feedbacks: the key role of sea ice and Snow in the polar and global climate system) and from the Academy of Finland for the project IMICROBE: Iron limitation on primary productivity in the Marginal Ice Zone of the Southern Ocean—unravelling the role of bacteria as mediators in the iron cycle (grant no. 335692). DL received grant funding from the Australian Research Council (grants no. FT190100688 and SR200100008) and from the Australian Government through the Antarctic Science Collaboration Initiative programme (grant ID ASCI000002).

References

Arrigo, K. R., Worthen, D. L., Lizotte, M. P., Dixon, P., and Dieckmann, G.: Primary production in Antarctic sea ice, *Science*, 276, 394–397, 1997.

Ayres, H. C., Ferreira, D., Park, W., Kjellsson, J., and Ödalen, M.: A comparison of the atmospheric response to the Weddell Sea Polynya in atmospheric general circulation models of varying resolutions, *Weather Clim. Dynam.*, 5, 805–820, 2024.

https://doi.org/10.5194/egusphere-2025-6509
Preprint. Discussion started: 10 February 2026

Boyd, P. W., Arrigo, K. R., Ardyna, M., et al.: The role of biota in the Southern Ocean carbon cycle, *Nat. Rev. Earth Environ.*, 5, 390–408, 2024.

Death, R., Wadham, J. L., Monteiro, F., Le Brocq, A. M., Tranter, M., Ridgwell, A., Dutkiewicz, S., and Raiswell, R.: Antarctic ice sheet fertilises the Southern Ocean, *Biogeosciences*, 11, 2635–2643, 2014.

de Jong, J., Schoemann, V., Maricq, N., Mattielli, N., Langhorne, P., Haskell, T., and Tison, J.-L.: Iron in land-fast sea ice of McMurdo Sound derived from sediment resuspension and wind-blown dust and its attribution to primary productivity in the Ross Sea, Antarctica, *Mar. Chem.*, 157, 24–40, 2013.

Drucker, R., Martin, S., and Moritz, R.: Observations of ice thickness and frazil ice in the St. Lawrence Island polynya from satellite imagery, upward looking sonar, and salinity/temperature moorings, *J. Geophys. Res.*, 108, C5, 3149, 2003.

Duprat, L., Bigg, G., and Wilton, D.: Enhanced Southern Ocean marine productivity due to fertilization by giant icebergs, *Nat. Geosci.*, 9, 219–221, 2016.

Edwards, R., and Sedwick, P.: Iron in East Antarctic snow: Implications for atmospheric iron deposition and algal production in Antarctic waters, *Geophys. Res. Lett.*, 28, 3907–3910, 2001.

Eicken, H., and Lange, M. A.: Development and properties of sea ice in the coastal regime of the southeastern Weddell Sea, *J. Geophys. Res.*, 94, 8193–8206, 1989.

Eicken, H., Lensu, M., Leppäranta, M., Tucker III, W. B., Gow, A. J., and Salmela, O.: Thickness, structure, and properties of level summer multiyear ice in the Eurasian sector of the Arctic Ocean, *J. Geophys. Res.*, 100, 22697–22710, 1995.

Fons, S., Kurtz, N., and Bagnardi, M.: A decade-plus of Antarctic sea ice thickness and volume estimates from CryoSat-2 using a physical model and waveform fitting, *The Cryosphere*, 17, 2487–2508, 2023.

Garrison, D. L., Close, A. R., and Reimnitz, E.: Algae concentrated by frazil ice: Evidence from laboratory experiments and field measurements, *Antarct. Sci.*, 1, 313–316, 1989.

Genovese, C., Grotti, M., Ardini, F., Corkill, M. J., Duprat, L. P., Wuttig, K., Townsend, A. T., and Lannuzel, D.: A proposed seasonal cycle of dissolved iron-binding ligands in Antarctic sea ice, *Elementa*, 10, 00030, 2022.

Gerringa, L. J. A., Alderkamp, A. C., Laan, P., Thuroczy, C. E., De Baar, H. J. W., Mills, M. M., van Dijken, G. L., van Haren, H., and Arrigo, K. R.: Iron from melting glaciers fuels phytoplankton blooms in the Amundsen Sea (Southern Ocean): Iron biogeochemistry, *Deep-Sea Res. II*, 71–76, 16–31, 2012.

https://doi.org/10.5194/egusphere-2025-6509
Preprint. Discussion started: 10 February 2026

Gow, A. J., Ackley, S. F., Weeks, W. F., and Govoni, J. W.: Physical and structural characteristics of Antarctic sea ice, *Ann. Glaciol.*, 3, 113–117, 1982.

Gradinger, R., and Ikävalko, I.: Organism incorporation into newly forming Arctic sea ice in the Greenland Sea, *J. Plankton Res.*, 20, 871–886, 1998.

Haumann, F. A., Moorman, R., Riser, S. C., Smedsrud, L. H., Maksym, T., Wong, A. P. S., et al.: Supercooled Southern Ocean waters, *Geophys. Res. Lett.*, 47, e2020GL090242, 2020.

Hersbach, H., Bell, B., Berrisford, P., et al.: The ERA5 global reanalysis, *Q. J. R. Meteorol. Soc.*, 146, 1999–2049, 2020.

Ito, M., Ohshima, K. I., Fukamachi, Y., Hirano, D., Mahoney, A. R., Jones, J., et al.: Favorable conditions for suspension freezing in an Arctic coastal polynya, *J. Geophys. Res. Oceans*, 124, 8701–8719, 2019.

Ito, M., Ohshima, K. I., Fukamachi, Y., Mizuta, G., Kusumoto, Y., and Kikuchi, T.: Underwater frazil ice and its suspension depth detected from ADCP backscatter data around the sea ice edge in the Sea of Okhotsk, *Cold Reg. Sci. Technol.*, 192, 103388, 2021.

Ito, M., Ohshima, K. I., Fukamachi, Y., Mizuta, G., Kusumoto, Y., and Nishioka, J.: Observations of frazil ice formation and upward sediment transport in the Sea of Okhotsk: A possible mechanism of iron supply to sea ice, *J. Geophys. Res. Oceans*, 122, 788–802, 2017.

Janssens, J., Meiners, K. M., Townsend, A. T., and Lannuzel, D.: Organic matter controls of iron incorporation in growing sea ice, *Front. Earth Sci.*, 6, 22, 2018.

Jeffries, M. O., Morris, K., Weeks, W. F., and Worby, A. P.: Seasonal variations in the properties and structural composition of sea ice and snow cover in the Bellingshausen and Amundsen Seas, Antarctica, *J. Glaciol.*, 43, 138–151, 1997.

Josey, S. A., Meijers, A. J. S., Blaker, A. T., et al.: Record-low Antarctic sea ice in 2023 increased ocean heat loss and storms, *Nature*, 636, 635–639, 2024.

Lancelot, C., Montety, A., Goosse, H., Becquevort, S., Schoemann, V., Pasquer, B., and Vancoppenolle, M.: Spatial distribution of the iron supply to phytoplankton in the Southern Ocean: A model study, *Biogeosciences*, 6, 2861–2878, 2009.

Lange, M. A., and Eicken, H.: Textural characteristics of sea ice and the major mechanisms of ice growth in the Weddell Sea, *Ann. Glaciol.*, 15, 210–215, 1991.

https://doi.org/10.5194/egusphere-2025-6509
Preprint. Discussion started: 10 February 2026

Lannuzel, D., Schoemann, V., de Jong, J. T. M., Tison, J.-L., and Chou, L.: Distribution and biogeochemical behaviour of iron in East Antarctic sea ice, *Mar. Chem.*, 106, 18–32, 2007.

Lannuzel, D., Schoemann, V., de Jong, J., Pasquer, B., van der Merwe, P., Masson, F., Tison, J.-L., and Bowie, A.: Distribution of dissolved iron in Antarctic sea ice: Spatial, seasonal, and inter-annual variability, *J. Geophys. Res.*, 115, G03022, 2010.

Lannuzel, D., van der Merwe, P. C., Townsend, A. T., and Bowie, A. R.: Size fractionation of iron, manganese and aluminium in Antarctic fast ice reveals a lithogenic origin and low iron solubility, *Mar. Chem.*, 161, 47–56, 2014.

Lannuzel, D., Grotti, M., Abelmoschi, M. L., and van der Merwe, P.: Organic ligands control the concentrations of dissolved iron in Antarctic sea ice, *Mar. Chem.*, 174, 120–130, 2015.

Lannuzel, D., Vancoppenolle, M., van der Merwe, P., de Jong, J., Meiners, K. M., Grotti, M., Nishioka, J., and Schoemann, V.: Iron in sea ice: Review and new insights, *Elementa*, 4, 000130, 2016.

Martin, J. H., Fitzwater, S. E., and Gordon, R. M.: Iron deficiency limits phytoplankton growth in Antarctic waters, *Global Biogeochem. Cycles*, 4, 5–12, 1990.

Martin, S.: Frazil ice in rivers and oceans, *Annu. Rev. Fluid Mech.*, 13, 379–397, 1981.

McPhee, M. G.: Ice–ocean momentum transfer for the AIDJEX ice model, *AIDJEX Bull.*, 29, 93–111, 1975.

Ohshima, K. I., et al.: Dominant frazil ice production in the Cape Darnley polynya leading to Antarctic Bottom Water formation, *Sci. Adv.*, 8, eadc9174, 2022.

Omstedt, A., and Svensson, U.: Modeling supercooling and ice formation in a turbulent Ekman layer, *J. Geophys. Res.*, 89, 735–744, 1984.

Parkinson, C. L.: A 40-year record reveals gradual Antarctic sea ice increases followed by decreases at rates far exceeding the Arctic, *Proc. Natl. Acad. Sci. USA*, 116, 14414–14423, 2019.

Person, R., Vancoppenolle, M., and Aumont, O.: Iron incorporation from seawater into Antarctic sea ice: A model study, *Global Biogeochem. Cycles*, 34, e2020GB006665, 2020.

Raiswell, R., Benning, L. G., Tranter, M., and Tulaczyk, S.: Bioavailable iron in the Southern Ocean: The significance of the iceberg conveyor belt, *Geochem. Trans.*, 7, 1–9, 2008.

https://doi.org/10.5194/egusphere-2025-6509
Preprint. Discussion started: 10 February 2026

Reimnitz, E., Clayton, J. R., Kempema, E. W., Payne, J. R., and Weber, W. S.: Interaction of rising frazil with suspended particles: Tank experiments with applications to nature, *Cold Reg. Sci. Technol.*, 21, 117–135, 1993.

Roach, L. A., Dörr, J., Holmes, C. R., Massonnet, F., Blockley, E. W., Notz, D., et al.: Antarctic sea ice area in CMIP6, *Geophys. Res. Lett.*, 47, e2019GL086729, 2020.

Sedwick, P. N., and DiTullio, G. R.: Regulation of algal blooms in Antarctic shelf waters by the release of iron from melting sea ice, *Geophys. Res. Lett.*, 24, 2515–2518, 1997.

Sherwood, C. R.: Numerical model of frazil ice and suspended sediment concentrations and formation of sediment-laden ice in the Kara Sea, *J. Geophys. Res.*, 105, 14061–14080, 2000.

Skatulla, S., Audh, R. R., Cook, A., Hepworth, E., Johnson, S., Lupascu, D. C., et al.: Physical and mechanical properties of winter first-year ice in the Antarctic marginal ice zone along the Good Hope Line, *The Cryosphere*, 16, 2899–2925, 2022.

Skogseth, R., Nilsen, F., and Smedsrud, L. H.: Supercooled water in an Arctic polynya: Observations and modeling, *J. Glaciol.*, 55, 43–52, 2009.

Smedsrud, L. H.: Frazil-ice entrainment of sediment: Large-tank laboratory experiments, *J. Glaciol.*, 47, 461–471, 2001.

Smedsrud, L. H.: A model for entrainment of sediment into sea ice by aggregation between frazil-ice crystals and sediment grains, *J. Glaciol.*, 48, 51–61, 2002.

Smedsrud, L. H., and Skogseth, R.: Field measurements of Arctic grease ice properties and processes, *Cold Reg. Sci. Technol.*, 44, 171–183, 2006.

Smedsrud, L. H.: Grease-ice thickness parameterization, *Ann. Glaciol.*, 52, 77–82, 2011.

Smedsrud, L. H., and Martin, T.: Grease ice in basin-scale sea-ice–ocean models, *Ann. Glaciol.*, 56, 69, 2015.

Smoluchowski, M.: Mathematical theory of the kinetics of the coagulation of colloidal solutions, *Z. Phys. Chem.*, 92, 129–135, 1917.

Smith, S. D.: Coefficients for sea surface wind stress, heat flux, and wind profiles as a function of wind speed and temperature, *J. Geophys. Res.*, 93, 15467–15472, 1988.

Stokes, G. G.: On the effect of the internal friction of fluids on the motion of pendulums, *Trans. Camb. Philos. Soc.*, 9, 8–106, 1851.

https://doi.org/10.5194/egusphere-2025-6509
Preprint. Discussion started: 10 February 2026

Tagliabue, A., Mtshali, T., Aumont, O., Bowie, A. R., Klunder, M. B., Roychoudhury, A. N., and Swart, S.: A global compilation of dissolved iron measurements: Focus on distributions and processes in the Southern Ocean, *Biogeosciences*, 9, 2333–2349, 2012.

Tamura, T., Ohshima, K. I., and Nihashi, S.: Mapping of sea ice production for Antarctic coastal polynyas, *Geophys. Res. Lett.*, 35, L07606, 2008.

Tedesco, L., Vichi, M., Haapala, J., and Stipa, T.: A dynamic biologically active layer for numerical studies of the sea ice ecosystem, *Ocean Modell.*, 35, 89–104, 2010.

Tedesco, L., and Lannuzel, D.: Iron in Antarctic sea ice (v1.0.0) [data set], *Zenodo*, https://doi.org/10.5281/zenodo.10019286, 2023.

Tennekes, H., and Lumley, J. L.: *A first course in turbulence*, MIT Press, Cambridge, MA, 1994.

Thompson, L., Smith, M., Thomson, J., Stammerjohn, S., Ackley, S., and Loose, B.: Frazil ice growth and production during katabatic wind events in the Ross Sea, Antarctica, *The Cryosphere*, 14, 3329–3347, 2020.

Tison, J.-L., Maksym, T., Fraser, A. D., et al.: Physical and biological properties of early winter Antarctic sea ice in the Ross Sea, *Ann. Glaciol.*, 61, 241–259, 2020.

Tison, J.-L., Schwegmann, S., Dieckmann, G., Rintala, J.-M., Meyer, H., Moreau, S., and Delille, B.: Biogeochemical impact of snow cover and cyclonic intrusions on the winter Weddell Sea ice pack, *J. Geophys. Res. Oceans*, 122, 9548–9571, 2017.

van der Merwe, P., Lannuzel, D., Nichols, C. A. M., Meiners, K. M., Heil, P., Norman, L., Thomas, D. N., and Bowie, A. R.: Biogeochemical observations during the winter–spring transition in East Antarctic sea ice: Evidence of iron and exopolysaccharide controls, *Mar. Chem.*, 115, 163–175, 2009.

Wadley, M. R., Jickells, T. D., and Heywood, K. J.: The role of iron sources and transport for Southern Ocean productivity, *Deep-Sea Res. I*, 87, 82–94, 2014.

Wang, S., Bailey, D., Lindsay, K., Moore, J. K., and Holland, M.: Impact of sea ice on the marine iron cycle and phytoplankton productivity, *Biogeosciences*, 11, 4713–4731, 2014.

Weeks, W. F., and Ackley, S. F.: The growth, structure and properties of sea ice, *CRREL Monogr.*, 82–1, 1982.

https://doi.org/10.5194/egusphere-2025-6509
Preprint. Discussion started: 10 February 2026

582 Wilchinsky, A. V., Heorton, H. D. B. S., Feltham, D. L., and Holland, P. R.: Impact of ice formation in leads on sea ice mass
583 balance using a new frazil and grease ice parameterisation, *J. Phys. Oceanogr.*, 45, 2025–2047, 2015.

584 Zhang, Z., Xie, C., Castagno, P., et al.: Evidence for large-scale climate forcing of dense shelf water variability in the Ross
585 Sea, *Nat. Commun.*, 15, 8190, 2024.